Cool-SPS stabilization and sintering of thermally fragile, potentially magnetoelectric, NH4FeP2O7

Thomas Herisson de Beauvoir, Anna Sangregorio, A. Bertrand, Christophe Payen, Dominique Michau, U-Chan Chung, Michaël Josse

Version of Record: https://www.sciencedirect.com/science/article/pii/S0272884218334850
Manuscript_b1db1ecbb0aa84b674e6f210cbb3ca44

Cool-SPS stabilization and sintering of thermally fragile, potentially magnetoelectric, $NH_4FeP_2O_7$ (*CJ-3:IL04*)

T. Herisson de Beauvoir, A. Sangregorio, A. Bertrand, C. Payen, D. Michau, U-C. Chung, M. Josse*

Abstract

Cool-SPS conditions (low temperature/high pressure) can be used to densify materials with limited thermodynamical stability, due to low temperature phase transition, melting, decomposition… We recently demonstrated the potential of SPS for the stabilization and densification of diversified materials at very low temperatures. Here we report the sintering of a potentially magnetoelectric pyrophosphate with low temperature decomposition. Characterization of its magnetic properties are presented, and dielectric/magnetoelectric characterization could also be performed thanks to the high densification obtained at temperatures as low as 200 °C.

Introduction

Low temperature ceramic sintering techniques have recently been developed and showed extraordinary potential for accessing high density at extremely low temperatures, typically below 400 °C, including Cold Sintering Process [1–7], Hydrothermal Hot Pressing [8–10] and Cool-SPS [11,12]. Beyond the energy and cost reduction offered by temperature reduction [13], multiple gaps are bridged by such processes. Indeed, such low processing temperatures open new possibilities such as the formation of novel polymer/ceramic composite materials, with ceramic as a major phase [14–16]. This also enables the formation of novel LTCC materials [17]. Other perspectives have recently been recently explored in the case of Cool-SPS, highlighting additional advantages of these low temperature processing techniques. One of them lies in the applied pressure necessary to realize such processes. In prior works, we observed that materials stability ranges may be modified under applied mechanical pressure, enabling stabilization of thermodynamically fragile phases – such as compounds facing low temperature decomposition, melting or irreversible phase transition [12] – and their efficient sintering (by Cool-SPS) resulting in very high density (typically above 95% of theoretical density). Another one is the opportunity to use, and also sinter efficiently, hydrated precursors [12], by controlling the dehydration through optimized sintering cycles [11]. One may also be able to perform *in situ* synthesis of phases that cannot be synthesized quantitatively otherwise [12]. Such potentialities create an opportunity to diversify the chemicals classes of materials investigated for diverse properties (physical, chemical…). Exploring these low temperature processing techniques can also allow for breakthroughs such as the recent elaboration of the first molecular ceramic [18]. One can thus foresee the potential of low temperature sintering methods for

bridging processing gaps (elaboration at low temperature), chemical gaps (enabling investigation of more diversified families of compounds), or even shaping gaps (processing of molecular ceramics previously unknown).

Indeed, we are now able to obtain dense materials from powders that were up to now considered to be impossible to sinter, and thus characterized as powder, films or crystals, with the inherent processing demands and characterization limitations of these shapings[1]. Widening the span of sinterable materials opens up interesting opportunities, especially in sulfate and phosphate compounds. They usually show low temperature stability, making their processing more difficult than refractory oxides. This concerns various applications such as electronic properties for batteries [19] or even mechanical ones in the process of biomaterials [20]. Using Cool-SPS among these low temperature processing techniques, it was possible to highlight magnetoelectric properties of $MnSO_4$ ceramics that could not be obtained through conventional sintering [11]. When looking for magnetoelectric properties in single phase materials, it becomes interesting to use low temperature sintering techniques to densify materials which crystal-chemical and magnetic properties allow for a potential magnetoelectric coupling. In the present study, we focus our interest on $NH_4FeP_2O_7$, once reported for its structure [21]. It completes the series of iron pyrophosphates $AFeP_2O_7$ (A = Li, Na, K, Rb, Cs, Ag) [22–25], which display antiferromagnetic phase transitions below room temperature thanks to super-super exchange interactions [22]. $NH_4FeP_2O_7$ is also isostructural to $KCrP_2O_7$, a pyrophosphate which symmetry allows for a magnetoelectric coupling [26], and this is an indictment to explore similar properties in the title compound. The main challenge to test such a magnetoelectric coupling is to obtain a highly densified ceramic to allow for dielectric characterization and avoid spurious contributions related to poor densification. To reach this objective, we propose to use Cool-SPS an efficient technique to obtain both high density and phase stabilization [12].

Experimental section

$NH_4FeP_2O_7$ synthesis is performed through solid state reaction of a green pellet constituted of both $(NH_4)_2HPO_4$ (Sigma Aldrich 98%) and α-Fe_2O_3. The latter is obtained from the heat treatment of $Fe(NO_3)_3 \cdot 9H_2O$ (Sigma Aldrich 98%) at 500 °C overnight, as commercial α-Fe_2O_3 presents a poor reactivity and its use results in an important amount of non-reacted α-Fe_2O_3. The two powders are mixed in an agate mortar and pelletized, then they are fired in a furnace at 210 °C for 24h. Sealed nitrogen

[1] *The processing of films requires compatible methods and substrates, the growth of single crystals require specific methods and time, both can require multiple-step processing. Characterization methods requiring electrical contact, dense samples (i.e. dielectric measurements…) are generally impossible for powders. The characterization of films frequently require specific methods for data collection, analysis and interpretation. The characterization of crystal can be limited by their inherent anisotropy (except for the cubic crystal system) and growth habit (acicular growth, platelets…) and may require complex preparation steps (oriented cutting, polishing…).*

environment, as well as nitrogen flux, were used to perform the synthesis, but resulted in a high content of remaining iron oxide, and sometimes promoted the formation of other phosphates as secondary phases. Using a sealed primary vacuum atmosphere allowed to obtain the higher ratio of $NH_4FeP_2O_7$ over α-Fe_2O_3. When a stoichiometric ratio of $(NH_4)_2HPO_4$ and iron oxide is used, there is an important part of remaining iron oxide, due to the volatilization of ammonium phosphate. Adding an excess of $(NH_4)_2HPO_4$ allows to compensate this volatilization, up to a point were other phases appear. The best compromise was found to be a 20 wt.% excess of $(NH_4)_2HPO_4$, although traces of α-Fe_2O_3 are still visible on the XRD pattern of the as-synthesized product. After synthesis, the powder was placed in a SPS sintering die made of WC and surrounded by Ta foils to avoid any cross contamination between the die and the powder.

Dense ceramics were prepared with Spark plasma sintering (Dr. Sinter Lab spark plasma sintering system, Model SPS-511S/SPS-515S) in WC:Co 10 mm die using 0.5 g of powder for each sintering attempt. Thermocouple is used to monitor temperature, in contact with the inner part of the die. 12 ON/2 OFF pulse sequence is applied for all samples. Densification was continuously monitored by the displacement of a punch rod. A 30 °C/min heating ramp was used for all different sintering experiments, while temperature was varied from 200 °C to 300 °C. Pressure was set to 300 MPa and sintering time to 10 min for all samples. Sintering attempts were performed under primary vacuum of about 10 Pa. Powder and pellet diffraction were performed with a Phillips X'Pert MPD X-ray diffractometer with the Bragg–Brentano geometry using Cu Kα1/Kα2 radiation ($10° < 2\theta < 80°$ range, step of 0.017°). The ceramics' relative densities were evaluated by geometrical measurements considering a theoretical density of 2.75 g/cm^3 for $NH_4FeP_2O_7$ [21]. The pellets' microstructures were observed on fracture surfaces, with a scanning electron microscope (JEOL 840 SEM). TGA measurements were performed with a Setaram tag2400 apparatus. Magnetic measurements were performed with a MPMS-7-XL (S.Q.U.I.D) magnetometer (Quantum Design) on ceramics. Zero-field cooled and field cooled data were collected with an applied field of 1 kOe and with increasing temperature from 2K to 300K. Silver electrodes were deposited on both surfaces of the pellets and silver wires were subsequently used for sake of electrical connection. Once prepared for dielectric measurements, the ceramics were placed in a Quantum Design Physical Properties Measurement System (PPMS) from which a 9 T magnetic field can be applied. The dielectric measurements were carried out in the frequency range of $10^2 – 10^6$ kHz (the amplitude of the applied ac electric field being 1V) using an HP4194a impedance bridge, at heating and cooling rates between 0,2 and 1 K/min. Measurements of capacitance and dielectric losses were first performed by scanning temperature with and without application of a magnetic field of 9T. In a second step, the magnetic field was swept from -9T to 9T at 2K to evaluate the magnetoelectric behavior of the samples.

Results and discussion

XRD data confirm the structural model proposed in the literature [21], and points the difficulty to fully separate as-synthesized $NH_4FeP_2O_7$ phase from α-Fe_2O_3 (see figure 1a and b). Whatever the temperature conditions tested for synthesis, α-Fe_2O_3 traces remain present after synthesis of the powder. At temperatures higher than 210 °C, decomposition of the target pyrophosphate occurs, and other phosphates are formed. On the opposite, synthesis performed below 210 °C show a limited reactivity, leading to an important amount of remaining α-Fe_2O_3. Therefore, synthesis temperature was set to 210 °C, and 220 °C is considered as decomposition temperature under vacuum, and is reported on figure 1 c) as a dashed red line. Despite the presence of hematite in the powder, XRD profile refinements (see table 1) confirm that lattice parameters of $NH_4FeP_2O_7$ phase are consistent with literature data [21]. After the powder was synthesized, it was placed in a WC die to be sintered in Cool-SPS conditions. Sintering temperature ranging from 200 to 300 °C were used to prepare ceramics. Interestingly, it is observed that the contribution of α-Fe_2O_3 traces to XRD patterns is apparently suppressed, as its very presence after sintering can be doubted for ceramics prepared at 250°C and above (figure 1 a and b). An hypothesis for that observation deals with the presence of 20 wt.% of ammonium hydrogen phosphate during synthesis, which may remain unreacted, possibly in amorphous form. We know from XRD on as-synthesized powder that α-Fe_2O_3 remains in excess. Therefore, Cool-SPS treatment on the as-synthesized powder, in which some precursors remain, likely promotes their reactivity while sintering is performed, ultimately resulting in the formation of pure, crystalized $NH_4FeP_2O_7$ when Cool-SPS is performed at 300°C. This makes the present processing route a reactive sintering, which probably contributes to the high density obtained, despite the very low temperature used, down to 200 °C, even below the synthesis temperature. From table 1, we can confirm the preservation of $NH_4FeP_2O_7$ lattice parameters, thus phase purity. Table 1 also displays densities of pellets sintered at temperatures ranging from 200 to 300 °C. All of them show a density above 94 %, even reaching 98 % for a 300 °C sintering treatment. Thanks to Cool-SPS efficiency, short sintering time (10 min only) and very low sintering temperatures are sufficient to obtain highly dense ceramic materials. These observations confirm the possibility of using SPS in such low temperature conditions, to extend the stability range of some compound, and to rely on reactive sintering in Cool-SPS conditions.

Moreover, considering thermal analysis performed on the initial powder (figure 1c), decomposition in air occurs in three steps ranging from 170 to 600 °C. The important information to consider in the present case it the starting decomposition temperature, 170 °C. This corresponds to 130 °C below the sintering temperature. However, we know from investigating its synthesis conditions that $NH_4FeP_2O_7$ is more stable under vacuum than in air. Decomposition temperature has previously been determined as 220 °C under vacuum. Considering now the highest sintering temperature used to obtain a 98% dense sample,

this represents 80 °C above the decomposition temperature under vacuum. It suggests a modified thermal stability range in Cool-SPS conditions compared to atmospheric pressure conditions, which has already been pointed out for other materials [12]. As the refined lattice parameters of the ceramics (table 1), obtained from profile refinements (figure 1 a), show very good consistency with the literature and from one sample to the other, it is clear that Cool-SPS processing above decomposition temperature preserves (and indeed increase) the phase purity from as-synthesized powder to 300 °C sintered ceramic of $NH_4FeP_2O_7$. This confirms the preservation of the phase 80 °C above its decomposition temperature in vacuum and allows using the obtained samples for further physical characterizations.

SEM images were taken on fractured pellets to observe their microstructure. According to these observation (figure 2), no open porosity is observed, and the high densifications geometrically measured are confirmed. Considering the quality of the pure and dense ceramics prepared, physical characterization can be performed on the sintered samples. In the following, all characterizations presented correspond to 300 °C sintered pellet, which is both the most dense and most pure specimen at our disposal. Since no magnetic characterization of $NH_4FeP_2O_7$ has been reported previously, the present work is an opportunity to complete the data concerning the $AFeP_2O_7$ series (A = Li, Na, K, Rb, Cs, Ag). Figure 3 displays zero field cool magnetic measurement revealing a maximum of magnetization of 0.17 $emu.g^{-1}$ at 21 K, and thus a transition to an antiferromagnetic phase below that point. The Curie-Weiss fit perfectly describes the sample magnetic behaviour at high temperature in the paramagnetic state, with C = 1.19 $emu.K.mol^{-1}$ and θ = -32.9 K, confirming the antiferromagnetic nature of magnetic interactions in $NH_4FeP_2O_7$. These observations are consistent with literature data on $AFeP_2O_7$ (A = Li, Na, K, Cs, Ag) [22–25], which are recalled in table 2 along with the contribution from this work. Most representatives of this series show antiferromagnetic transitions at low temperatures, and all of them present negative value of θ, indicative of antiferromagnetic interactions. Our data places the ammonium representative as the one displaying the weakest magnetic interactions in the series from this viewpoint, and also show that the magnetic behaviour in this series can not be rationalized on the basis of a simple crystal-chemical parameter such as ionic radius. Since high density pellets can be obtained after sintering, it is now possible to perform reliable dielectric measurements. Figure 4a presents the dielectric measurements performed on pellet sintered at 300 °C, which were found reproducible from several ceramics prepared in the same conditions. According to the small value of the permittivity and the low level of losses (below 0.01), we can tell that the quality of grain boundaries is very good, as defect-related contributions from grain boundaries would otherwise clearly dominate the dielectric response of the sample. A relaxation is observed in the losses from 150 to 100 K, which is associated with a slight decrease in the real part of permittivity. However, the mechanism associated with this dielectric anomaly has not been identified yet, and the small amplitude of permittivity evolution prevents deeper analyses to identify it. As $NH_4FeP_2O_7$ crystal symmetry allows for

a magnetoelectric coupling [26] it is worth trying to investigate it through magnetic field dependent dielectric measurements. On figure 4b is displayed the dependence of dielectric permittivity to applied magnetic field, at 300 kHz and 2 K for the same sample. As can be observed from the plot, a dependence is measured, mostly between ±3 to ±6T, which remains of rather small amplitude, preventing us from performing additional characterization (such as magnetic field dependent polarization) and concluding on its nature. Anyway, this points out the possible presence of a magnetoelectric in the phase, which requires further investigations to be confirmed.

Conclusion

It was possible to synthesize $NH_4FeP_2O_7$ powder from solid state route, by firing diammonium hydrogen phosphate and iron oxide at 210°C under primary vacuum. However hematite α-Fe_2O_3 remains present after synthesis, while XRD confirms the stabilization of the target phase, with lattice parameters similar to those reported in the literature [21]. Among the key features of the present work is the behavior of this material during its processing by Cool-SPS. Although no literature data deal with the densification of this material, it was possible to obtain a highly dense material using temperature as low as 200 °C and sintering time as short as 10 min. This illustrates the potential of low temperature sintering techniques, such as Cool-SPS, for the elaboration of highly densified ceramics. As $NH_4FeP_2O_7$ decomposes in air around 170 °C and in vacuum around 220 °C, this also illustrates the possibility, pointed previously [12], to densify some thermodynamically fragile materials beyond their thermal stability range, and expand the range of possible characterizations to that allowed by ceramics, which are otherwise mostly limited to studies performed on powder or single-crystals. Moreover, in the present case, although the targeted phase could not be obtained as a pure powder after synthesis, Cool-SPS processing essentially removed the α-Fe_2O_3 excess, most probably thanks to reactive sintering. Finally, obtaining such phase-pure, high-density pellets allowed to perform physical characterizations. Magnetic measurements revealed an antiferromagnetic phase transition at 21 K, consistent with literature data on other members of $AFeP_2O_7$ (A = Li, Na, K, Cs, Ag) family showing similar properties. Dielectric properties could be measured on dense pellet, confirming the quality of grain boundaries and exhibiting a dielectric anomaly in the range 100-150 K. In parallel, magnetic dependence of permittivity exhibits a clue for magnetoelectric coupling in $NH_4FeP_2O_7$, which needs to be further investigated.

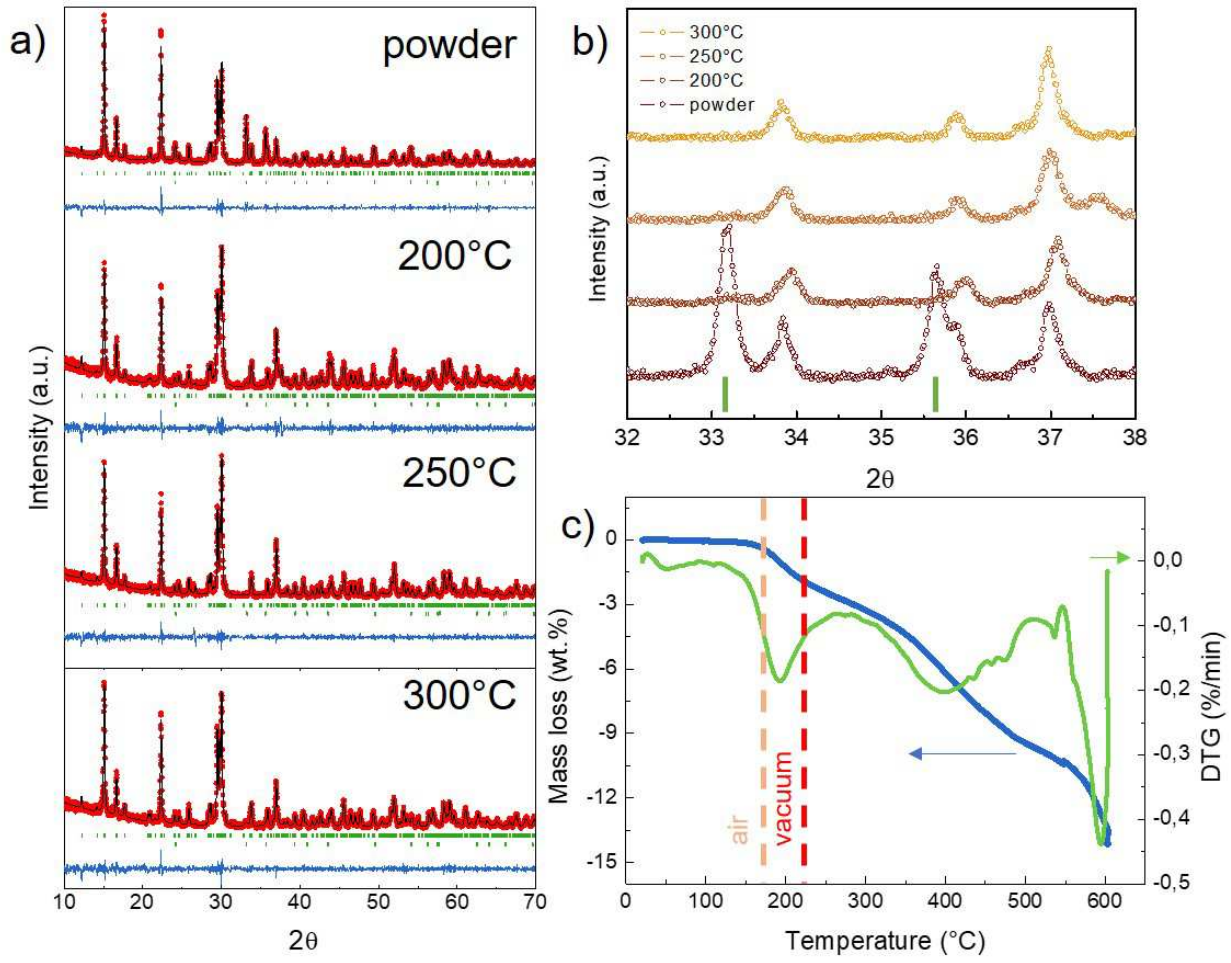

Figure 1: a) XRD patterns collected on synthetized powder and sintered pellets at various temperatures ; b) zoom in the region of $32° \leq 2\theta \leq 38$, with a green mark representing Bragg positions for Fe_2O_3 hematite phase (other contributions are due to the title compound) ; c) TGA in air at constant heating rate of 5 °C/min from room temperature to 600 °C on $NH_4FeP_2O_7$ powder after synthesis (blue line correspond to TG data and green line to dTG), dashed orange line represents the starting decomposition temperature in air extracted from TGA(170 °C) while red dashed line represents the stability temperature observed in primary vacuum, obtained from synthesis (220 °C)

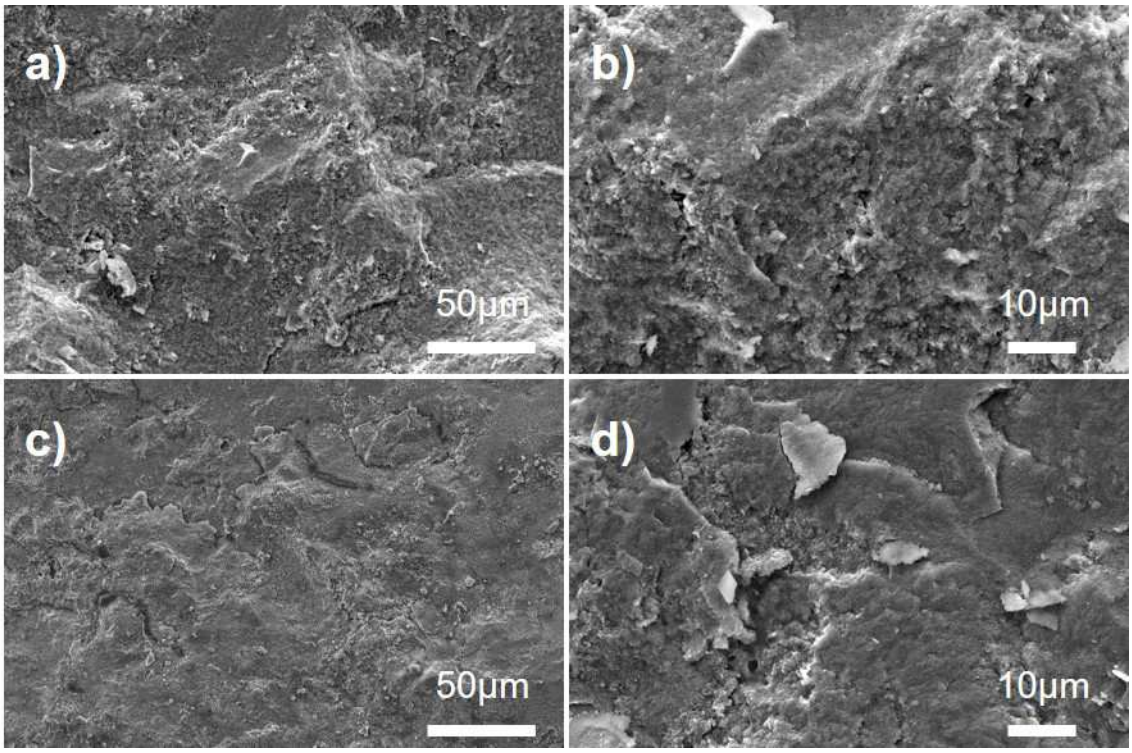

197

198 *Figure 2: SEM images of fractured samples sintered at (a-b) 200 °C and (c-d) 300 °C*

199

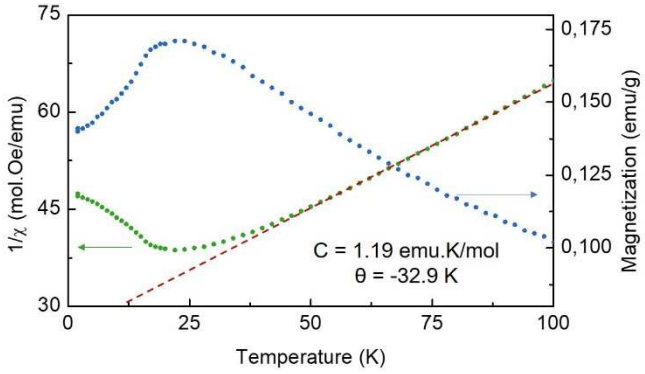

200

201 *Figure 3: Zero field cool measurement on pellet sintered at 300 °C - 300 MPa - 10 min, green dots correspond to inverse of*
202 *magnetic susceptibility and blue dots to sample magnetization ; red dashed line corresponds to Curie-Weiss fit*

203

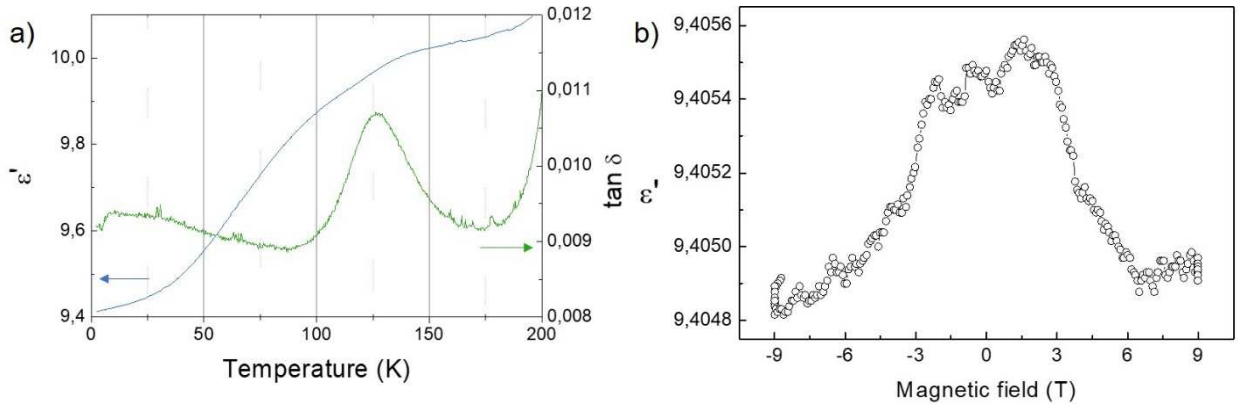

Figure 4: a) Dielectric measurement in the range 2 – 200K, measured at 300 kHz min and b) Magnetic field dependence of permittivity at 300 kHz measured on a pellet sintered at 300 °C - 300 MPa - 10

Table 1: Refined lattice parameters for powder and pellets sintered at various temperatures

Sample	Sintering temperature (°C)	a (Å)	b (Å)	c (Å)	β (°)	Relative density (%)
#1	200	7.5175(3)	10.0065(3)	8.2738(3)	105.895(3)	94.1(5)
#2	250	7.5180(2)	10.0055(3)	8.2780(2)	105.901(3)	95.6(5)
#3	300	7.5176(2)	10.0043(2)	8.2729(2)	105.900(3)	98.0(5)
Powder	-	7.5197(4)	10.0023(5)	8.2759(5)	105.856(6)	-
Reference [20]	-	7.5219(2)	10.0018(3)	8.2729(3)	105.887(3)	-

Table 2: Comparison of some crystal-chemical and magnetic data for the pyrophosphate series $M^IFeP_2O_7$ (M^I=Na, K, Cs, NH_4, Ag).

Compound	Space group	θ (K)	R_A (Å)	Ref.
$NaFeP_2O_7$	$P2_1/c$	–53	1,18	[23]
$AgFeP_2O_7$	$P2_1/c$	–165.9	1,28	[22]
$KFeP_2O_7$	$P2_1/c$	–90	1,51	[23]
$NH_4FeP_2O_7$	**$P2_1/c$**	**–32.9**	**1,55**	**This Work**
$CsFeP_2O_7$	$P2_1/c$	–64.9	1,74	[25]

[1] J.-P. Maria, X. Kang, R.D. Floyd, E.C. Dickey, H. Guo, J. Guo, A. Baker, S. Funihashi, C.A. Randall, Cold sintering: Current status and prospects, J. Mater. Res. 32 (2017) 3205–3218.

[2] H. Guo, A. Baker, J. Guo, C.A. Randall, Protocol for Ultralow-Temperature Ceramic Sintering: An Integration of Nanotechnology and the Cold Sintering Process, ACS Nano. 10(11) (2016) 10606–10614.

[3] S. Funahashi, J. Guo, H. Guo, K. Wang, A.L. Baker, K. Shiratsuyu, C.A. Randall, Demonstration of the Cold Sintering Process Study for the Densification and Grain Growth of ZnO Ceramics, J. Am. Ceram. Soc. 100 (2017) 546–553.

[4] S.S. Berbano, J. Guo, H. Guo, M.T. Lanagan, C.A. Randall, Cold sintering process of Li1.5Al0.5Ge1.5(PO4)3 solid electrolyte, J. Am. Ceram. Soc. 100 (2017) 2123–2135.

[5] D. Wang, D. Zhou, S. Zhang, Y. Vardaxoglou, W. Whittow, D. Cadman, I. Reaney, Cold-Sintered Temperature Stable Na0.5Bi0.5MoO4-Li2MoO4 Microwave Composite Ceramics, ACS Sustain. Chem. Eng. 6 (2018) 2438–2444.

[6] I.J. Induja, M.T. Sebastian, Microwave dielectric properties of mineral sillimanite obtained by conventional and cold sintering process, J. Eur. Ceram. Soc. 37 (2017) 2143–2147.

[7] H. Guo, A. Baker, J. Guo, C.A. Randall, Cold Sintering Process: A Novel Technique for Low-Temperature Ceramic Processing of Ferroelectrics, J. Am. Ceram. Soc. 99 (2016) 3489–3507.

[8] A. Ndayishimiye, S. Buffière, M.A. Dourges, A. Largeteau, M. Prakasam, S. Mornet, O. Kaman, J. Zdeněk, J. Hejtmánek, G. Goglio, Design of 0–3 type nanocomposites using hydrothermal sintering, Scr. Mater. 148 (2018) 15–19.

[9] A. Ndayishimiye, A. Largeteau, M. Prakasam, S. Pechev, M.A. Dourges, G. Goglio, Low temperature hydrothermal sintering process for the quasi-complete densification of nanometric α-quartz, Scr. Mater. 145 (2018) 118–121.

[10] A. Ndayishimiye, A. Largeteau, S. Mornet, M. Duttine, M.-A. Dourges, D. Denux, M. Verdier, M. Goune, T. Herisson de Beauvoir, C. Elissalde, G. Goglio, Hydrothermal Sintering for Densification of Silica . Evidence for the Role of Water, J. Eur. Ceram. Soc. 38 (2018) 1860–1870.

[11] T. Herisson de Beauvoir, F. Molinari, U.-C. Chung-Seu, D. Michau, D. Denux, M. Josse, Densification of MnSO4 ceramics by Cool-SPS: evidences for a complex sintering mechanism and magnetoelectric coupling, J. Eur. Ceram. Soc. 38 (2018) 3867–3874.

[12] T. Herisson de Beauvoir, A. Sangregorio, I. Cornu, C. Elissalde, M. Josse, Cool-SPS: an opportunity for low temperature sintering of thermodynamically fragile materials, J. Mater. Chem. C. 6(9) (2018) 2229–2233.

[13] D. Sohrabi Baba Heidary, M. Lanagan, C.A. Randall, Contrasting energy efficiency in various ceramic sintering processes, J. Eur. Ceram. Soc. 38 (2018) 1018–1029.

[14] X. Zhao, J. Guo, K. Wang, T. Herisson De Beauvoir, B. Li, C.A. Randall, Introducing a ZnO-PTFE (Polymer) Nanocomposite Varistor via the Cold Sintering Process, Adv. Eng. Mater. (2018) 1700902.

[15] J. Guo, H. Guo, D.S.B. Heidary, S. Funahashi, C.A. Randall, Semiconducting properties of cold sintered V2O5 ceramics and Co-sintered V2O5-PEDOT:PSS composites, J. Eur. Ceram. Soc. 37 (2016) 1529–1534.

[16] J. Guo, S.S. Berbano, H. Guo, A.L. Baker, M.T. Lanagan, C.A. Randall, Cold Sintering Process of Composites : Bridging the Processing Temperature Gap of Ceramic and Polymer Materials, Adv. Funct. Mater. 26 (2016) 7115–7121.

[17] S. Funahashi, H. Guo, J. Guo, A.L. Baker, K. Wang, K. Shiratsuyu, C.A. Randall, Cold sintering and co-firing of a multilayer device with thermoelectric materials, J. Am. Ceram. Soc. 100 (2017) 3488–3496.

[18] T. Herisson de Beauvoir, V. Villemot, M. Josse, On the first molecular ceramic, obtained by Cool-SPS, submitted.

[19] X. Fleury, M.H. Noh, S. Geniès, P.X. Thivel, C. Lefrou, Y. Bultel, Fast-charging of Lithium Iron Phosphate battery with ohmic-drop compensation method: Ageing study, J. Energy Storage. 16 (2018) 21–36.

[20] D. Grossin, S. Rollin-Martinet, C. Estournès, F. Rossignol, E. Champion, C. Combes, C. Rey, C. Geoffroy, C. Drouet, Biomimetic apatite sintered at very low temperature by spark plasma sintering: Physico-chemistry and microstructure aspects, Acta Biomater. 6 (2010) 577–585.

[21] B.F. Alfonso, J.A. Blanco, M.T. Fernández-Díaz, C. Trobajo, S.A. Khainakov, J.R. García, On the crystal structure and thermal decomposition of ammonium-iron(iii) bis(hydrogenphosphate), Dalt. Trans. 39 (2010) 1791–1796.

[22] K. V. Terebilenko, A.A. Kirichok, V.N. Baumer, M. Sereduk, N.S. Slobodyanik, P. Gütlich, Structure and magnetic properties of AgFeP2O7, J. Solid State Chem. 183 (2010) 1473–1476.

[23] D. Riou, N. Nguyen, R. Benloucif, B. Raveau, LiFeP2O7 : Structure and magnetic properties, Mater. Res. Bull. 25 (1990) 1363–1369.

[24] T. Moya-Pizarro, R. Salmon, L. Fournes, G. Le Flem, B. Wanklyn, P. Hagenmuller, Etudes cristallographique magnétique et par résonance Mössbauer de la variété de haute température du pyrophosphate NaFeP2O7, J. Solid State Chem. 53 (1984) 387–397.

[25] E. Dvoncova, K.-H. Lii, Synthesis, crystal structure, and magnetic susceptibilities of CsFeP2O7 and RbFeP2O7, J. Solid State Chem. 105 (1993) 279–286.

[26] S. Gentil, D. Andreica, M. Lujan, J. Rivera, F. Kubel, H. Schmid, Synthesis, structure and magnetic susceptibility of KCrP2O7 , a potential antiferromagnetic magnetoelectric, Ferroelectrics. 204 (1997) 35–44.